J. Condensed Matter Nucl. Sci. 38 (2024) 186–195

Research Article

Excess Heat in Nanoparticles of Nickel Alloys in Hydrogen

Jean-Paul Biberian, Robert Michel
VEGATEC, France

Christophe Le Roux
CNRS France

Mathieu Valat
University of Szczecin, Institute of Physics, Poland, and also with Sart von Rohr, France

Sébastien Bucher
LIFCO France

Arnaud Kodeck
Lakoco, Belgium

Per J.R. Sjöberg
Uppsala University, Sweden

Jacques Ruer
Sart von Rohr, France

Damien Chaudanson
Aix Marseille University, CNRS, CINAM, Marseille, France

Abstract

We have developed new kinds of materials made of nanoparticles of nickel-based alloys that show production of anomalous heat in an atmosphere of hydrogen. These materials are produced starting from hydrotalcite acting as precursors of nickel and nickel alloys supported on an amorphous alumina phase. The experiments are performed in a custom-made heat-flow calorimeter having a precision of $+/-100$ mW from room temperature up to 950°C. This report shows that excess heat is produced when hydrogen is introduced into the reaction cell, however more excess heat is measured when the hydrogen is pumped out.

Keywords: Energy, hydrotalcite, nickel, high temperature calorimetry

© 2023 ICCF. All rights reserved. ISSN 2227-3123

1. Introduction

In the framework of the European Project CleanHME, we worked on experiments using nanoparticles made of nickel-based compounds. These nano particles are of prime importance because previous experiments dating back to the work of Arata [1] using palladium nanoparticles embedded in zirconium oxide in a deuterium atmosphere show excess heat production with the sole excitation of heat. Takahashi et al. [2] have shown that such nickel and copper-based nano powders produce anomalous heat in hydrogen or deuterium. To measure accurately the heat produced we used a heat-flow calorimeter of Calvet type (also known as Seebeck) to reach high temperatures using low heating power. We have also developed a new method to produce nickel-based nano particles using a much cheaper technique than the one of Arata [1] and Takahashi et al. [2], using hydrotalcites as precursors. This new method allows us to produce large quantities of materials at low cost. In addition to the work with hydrotalcite, we have also studied thin films of nickel deposited on carbon powders.

2. The Calorimeter

In a standard Calvet calorimeter [3]–[5], the hot core is surrounded by a box which has an insulated wall equipped with thousands of thermocouples in series, alternatively placed on one side of the insulated wall and on the other side. Since the insulated wall is all around the heat source, all the heat produced by the hot core must go through the wall. The voltage at both ends of the series of thermocouples is a function of the core power source. This type of calorimeter is very insensitive to the position or the temperature of the heat source in the box.

We have developed a simplified Calvet calorimeter. In our design, shown in Figure 1, the heated quartz tube is filled with the active powder. The quartz tube is placed inside a vacuum chamber (stainless steel 150 mm long $\times$ 63 mm in diameter, see Figure 1b) itself surrounded by insulating material. The heat flow produced by the cell goes through the insulation layer and creates a temperature gradient across this thermal insulation. However, our design differs from the ideal Calvet calorimeter two-fold. Firstly, since the calorimeter and the quartz cell have a cylindrical geometry, therefore, it is not necessary to have thermocouples placed in all directions. Fifty thermocouples are in one plane, because of the cylindrical symmetry, the voltage measured is proportional to the voltage measured if there were thermocouples all around the cell. Secondly, there is no thermocouple on the top flange of the calorimeter, so the heat lost by the top flange is not taken into account. This loss is minimized by putting insulating material above the flange. If the room temperature of the laboratory is constant, then by calibration, this loss is the same for a blank run as an active experiment. Therefore, after calibration, the voltage measured with the 50 thermocouples is a good representation of the heat produced.

The quartz cell is heated by a Kanthal wire wrapped around it and covered by cement, as shown in Figure 1d. Three concentric stainless-steel screens are placed around the cell, inside the vacuum chamber, to reduce the heat lost by radiation, hence limiting the heating power required to reach a high temperature. The vacuum chamber is positioned inside the double wall cylindrical aluminum vessel. The heat resistant material is crossed by 50 type-K thermocouples connected in series, alternatively sealed on each side of the insulation material. Finally, the calorimeter is placed in a constant temperature water bath, as shown in Figure 1e. Temperatures up to 950°C can be reached.

We used two types of quartz cells, 90 $\times$ 20 mm cells heated from the outside with a Kanthal heating wire, and 90 $\times$ 40 mm quartz cells heated from inside (see Figure 2). The data acquisition and control system (DACS) capture and monitors measurements in the calorimeter. The DACS is responsible for acquiring temperatures, pressures, and the Seebeck signal from the thermocouples. Additionally, the DACS controls the electrical input power from a TDK Lambda power supply. This comprehensive system ensures accurate and reliable data collection while providing seamless control over the input power for the experimental setup.

Calibration of the calorimeter was made with a quartz cell filled with alumina powder in hydrogen, see Figure 3. The heating power was increased by 10 W steps up to 70 W. The input power is plotted against the voltage measured

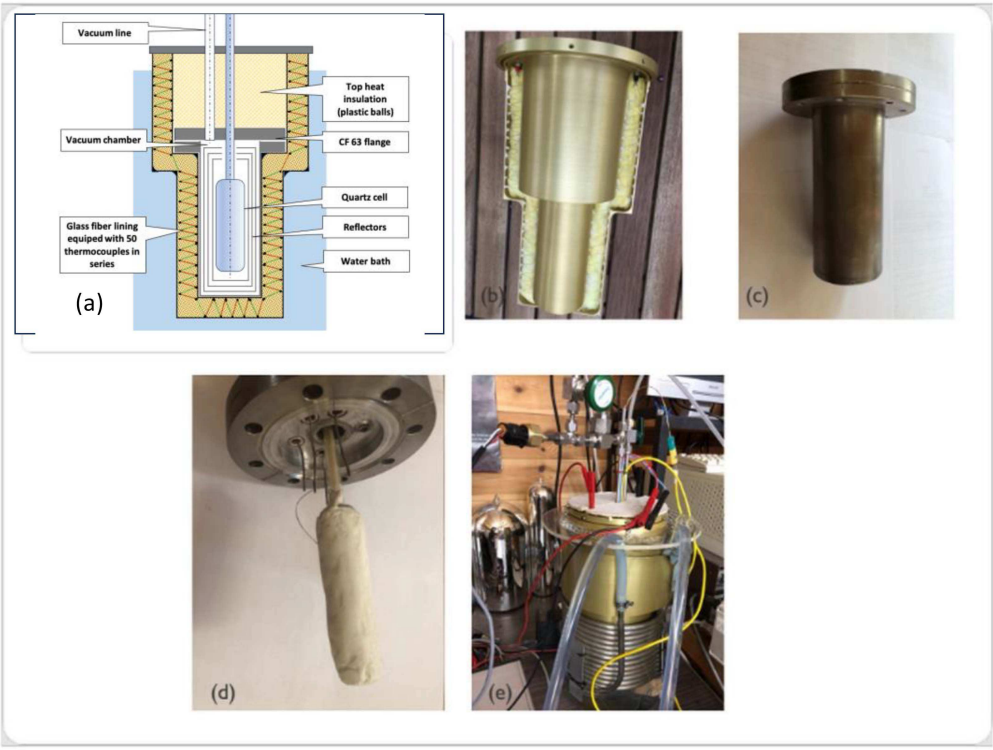

Figure 1. a) Schematic view of the calorimeter; b) Photo of the 50 thermocouples attached to the inner and outer cylinders; c) The 63 mm in diameter vacuum chamber with a CF63 flange; d) A 9 cm $\times$ 2 cm quartz cell with a Kanthal wire heater covered with a high temperature cement; e) Photo of the calorimeter in the constant temperature water bath.

by the 50 thermocouples, and a third order polynomial fit is used to determine the relation between voltage and power (Figure 3).

The formula deduced from the calibration is used to check the power measured vs. temperature. Figure 4 shows the calibration curve of Figure 3 vs temperature. It shows that the resolution is better than $+/-$ 100 mW. A limitation of the resolution of the calorimeter is due to the variations in the room temperature. The calorimeter is not a full Calvet one, since the top flange heat is not taken into account in the heat measurement, and a variation in the room temperature brings inaccuracy in the measurements. A second identical calorimeter is being tested in a constant temperature room and should produce better precision.

3. The powder

The method used by Arata [1] to produce the nanoparticles is a complex metallurgical technique. They use a melt-spinning/splat-cooling method of the desired alloy of palladium/nickel/zirconium in an argon atmosphere which produces an amorphous film. The amorphous film is then oxidized in air at 450°C. The oxidation occurs preferably on the zirconium, leaving the palladium-nickel in the form of metal nanoparticles of 5–10 nm in diameter. This technique is

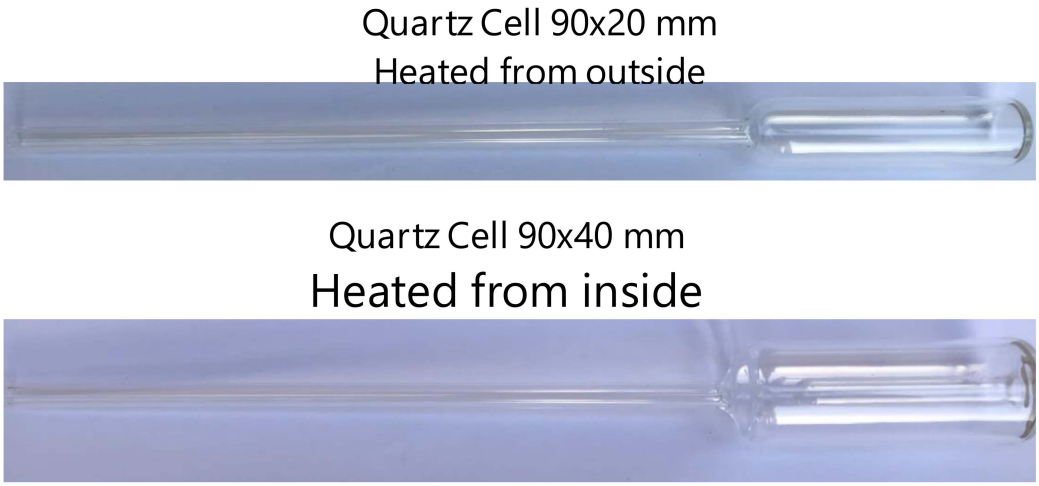

Figure 2. The two quartz cells.

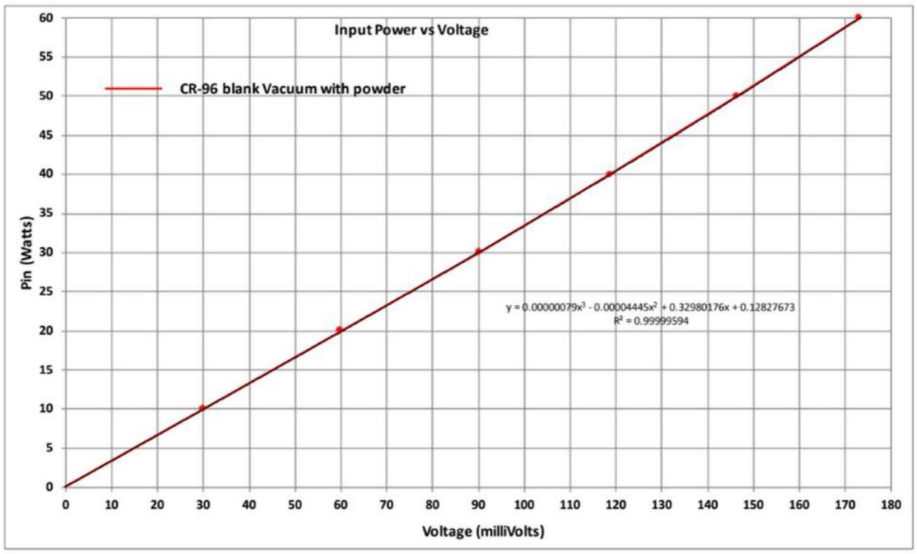

Figure 3. Input electrical power vs voltage measured with the 50 thermocouples in series.

used in the preparation of some catalysts [6]. However, these materials present some drawbacks with respect to their difficulty of preparation and/or cost.

In this study, a new method was developed to produce such metal nanoparticles supported on amorphous oxides. This method comprises the decomposition/reduction of an appropriate layered double hydroxide (LDH) [7] which is a class of minerals (natural and synthetic). The most abundant member on earth is the hydrotalcite whose formula is

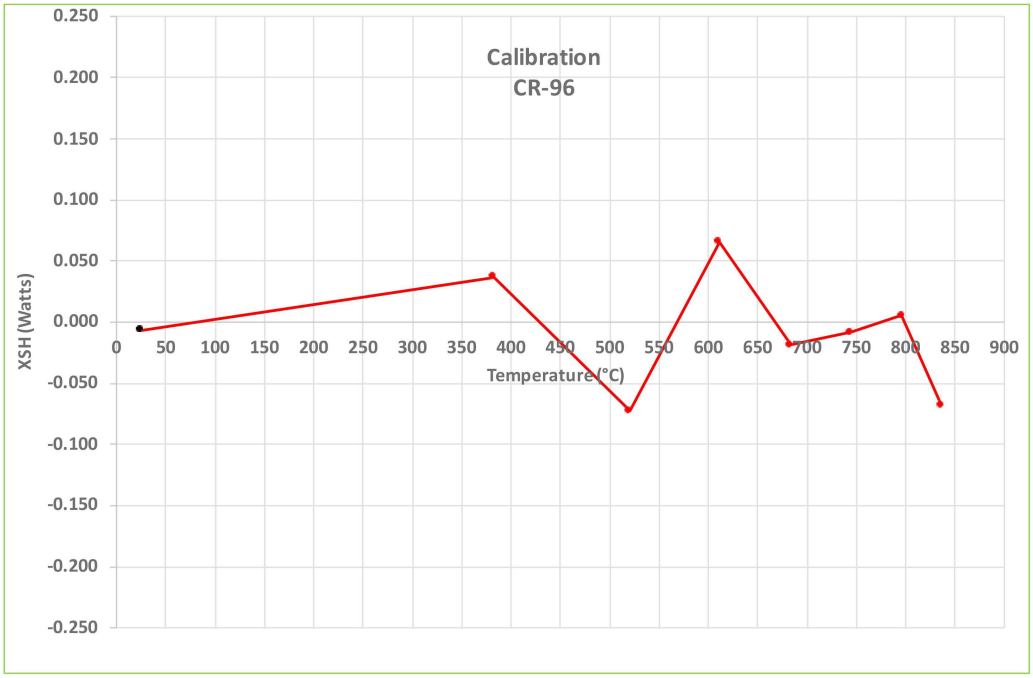

Figure 4. Calibration of the calorimeter filled with alumina powder in hydrogen up to 850°C.

$Mg_6Al_2(OH)_{16}CO_3$–$4H_2O$. Takovite, the hydrotalcite where magnesium has been replaced by nickel, has also been rarely found [8]. LDH can be represented by the general formula $[M^{II}{}_{1-x}\ M^{III}{}_x\ (OH)_2]^{x+}(A^{n-})_{x/n}$ hydrated with H_2O where i) M^{II} is a di-cation (Mg, Ni, Cu, Co, Zn, Fe, ...) and their mixtures in almost all proportions, ii) M^{III} is a tri-cation (Al, B, Ga, Fe, Y, ...) and their mixture in almost all proportions, iii) A is an anion ($CO_3{}^{2-}$, $NO_3{}^-$, Cl^-, ...), the most commonly found being carbonate. Additionally, other elements such as Zr and Ti can be incorporated in LDH crystalline structures. Under appropriate molar ratios of M^{II}, M^{III} and A, the chemical elements co-crystalize in a lamellar material called LDH. Mineral synthesis offers the unique opportunity to expand the scope of natural LDH. Thus, a wide variety of LDHs have been prepared by various methods [9], studied and designed for various applications [10], One of these applications is methanation (also known as Sabatier's reaction), a reaction involving hydrogen and CO_2 [11]. In this case, the synthetic LDH is used as a precursor to generate metal nanoparticles (mainly Ni) supported on amorphous alumina. A similar precursor has been reported to act as a pro-catalyst for the generation of hydrogen from N_2H_4-hydrate decomposition [12]. The thermal decomposition of such precursors involves successively i) a dehydration step, ii) a decarbonation step with release of CO_2, iii) a dehydroxylation step to end up with M^{II}-oxides supported on amorphous M^{III}-oxides. In the last step, conducted under hot hydrogen flow (300–700°C), the M^{II}/M^{III}-oxides are reduced to give the desired $M°/M^{III}$ metal-oxide mix (see Figure 5). Such material as prepared is then used for LENR experiments. This chemical method is easily scalable for industrial applications.

We start with synthetic hydrotalcites having the general formulas: $Ni_{5.25}Cu_{0.75}Al_2CO_3(OH)_{16}{\cdot}4(H_2O)$ and $Ni_6Al_2CO_3(OH)_{16}{\cdot}4(H_2O)$. In this work we used Ni/Cu 7/1 and pure nickel. The color of the original powder is green, and it is not magnetic (see the difference with the magnet in Fig. 5a and 5b). When the powder is heated under

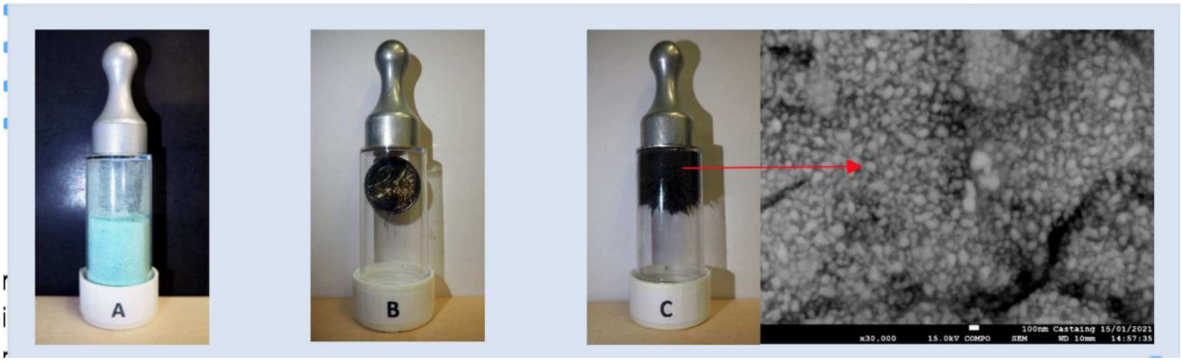

Figure 5. a) Original hydrotalcite Green not magnetic LDH $Ni_6Al_2CO_3(OH)_{16} - 4H_2O$; b) Magnet alone; c) Black Magnetic $Ni_6Al_2O_3$ attracted by the magnet, and Scanning Electron Microscopic view of nickel nanoparticles (white dots, but black at the naked eye).

vacuum up to 600°C, the color turns brown. It is still not magnetic. When the powder is heated under hydrogen, at 900°C, the powder becomes black and magnetic, as shown in Figure 5. In these conditions of operation, we did not observe any sintering.

4. Absorption of hydrogen in nickel

At room temperature, nickel does not absorb hydrogen at low pressure, because the reaction is endothermic. To introduce hydrogen in nickel, it is necessary to heat the material above 200°C [13]. Also of importance is the fact that hydrogen does not enter inside nickel if there is an oxide layer at its surface. Therefore, it is first necessary to reduce the oxide layer by heating in hydrogen before hydrogen can be absorbed by the metal nanoparticles. However, these two mechanisms are performed simultaneously. This behavior explains the procedure used in this work to produce excess power.

5. Experimental Results

5.1. Calorimetry

Experiments have been carried out in 2 cm and 4 cm diameter cells. We used hydrotalcites with Ni-Cu nanoparticles having the molar ratio 7/1 and pure nickel. The powder was either treated in a separate furnace under vacuum and hydrogen, or directly in the calorimeter. The initial powder (green) is heated under vacuum up to about 600°C (above this temperature in vacuum, there is formation of spinelles), then cooled down to room temperature. Experiments are performed at constant power with heating steps of 5 or 10 W either in vacuum or under hydrogen. The steps are continued until stabilization of the output power, typically 6 to 8 hours. At the maximum power, the cell is pumped down, and the power is lowered by steps again. The cycle of heating under hydrogen and cooling under vacuum is repeated until the excess power is stabilized. The maximum duration of an experiment at maximum temperature and under vacuum was four days, and produced close to 4 MJ of heat, with about 0.1 mole of metal.

An example of excess heat production is shown in Figure 6, with an hydrotalcite Ni-Cu with a molar ratio 7/1. The blue curve (CR-77A) corresponds to the first run under vacuum up to 390°C. At room temperature the cell is filled with hydrogen at a pressure of 1.3 Bars, and heated up to 547°C, (curve CR-77B). Most of the runs up to 600°C show excess energy of less that 200 mW. However, the green curve (CR-77C) in hydrogen shows an endothermic behavior between 330°C and 500°C. This type of behavior has been observed several times, but not systematically. It is of unknown origin at this point. We do not know if this is an artefact or a chemical or nuclear mechanism.

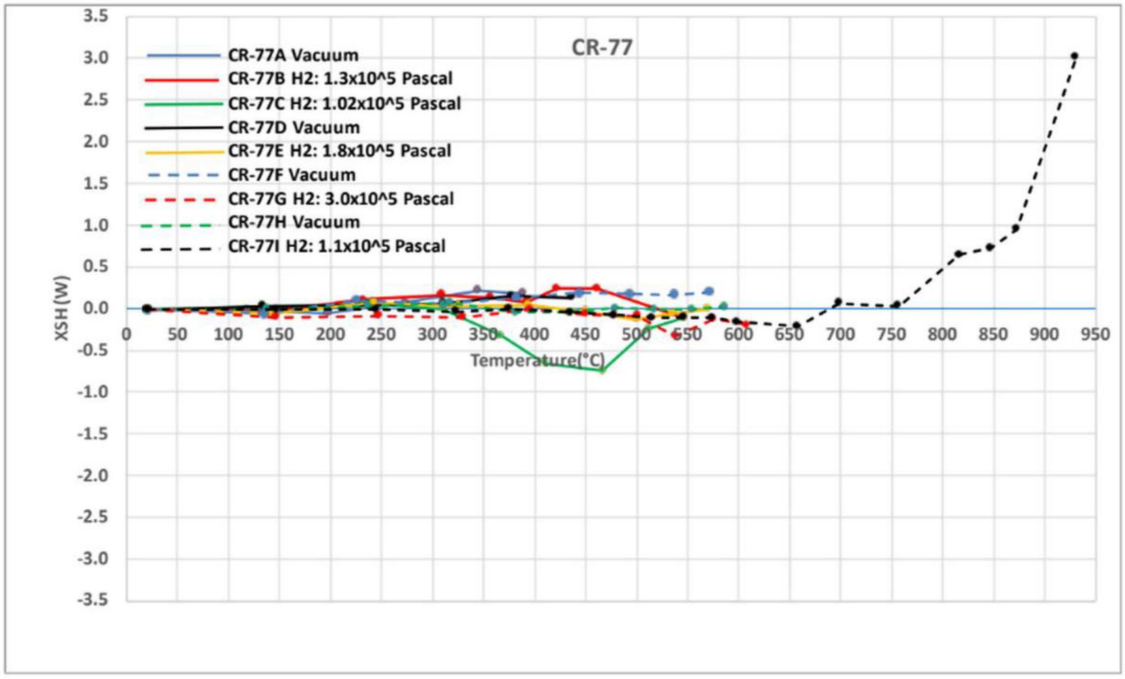

Figure 6. Experiment CR-77, example of production of excess heat with an hydrotalcite Ni-Cu ratio: 7/1 (14.6g).

Figure 7 shows the results of 7 experiments, 6 of them based on hydrotalcite, and one on nickel deposited on carbon powder. All of them show excess power at high temperatures. There are variations in the amount of excess heat observed, due to the various parameters that make each measurement unique: amount of material, preparation, and precision of the measurements. Another important point to be noted is that more excess power is measured after pumping out the hydrogen. After each cycle of loading hydrogen and pumping, the excess power increases. A saturation in the increase of excess heat happens after about four cycles.

5.2. Activation Energy

Because the experiments have been done at various temperatures it is possible to calculate the activation energy of the reactions. Figure 8 shows the various logarithmic plots of the excess energy vs 1/T. The activation energies vary from 0.6 eV to 1.8 eV. This is consistent with a diffusion of hydrogen atoms in the crystal lattices.

5.3. Transmutation?

In the experiment CR-92 with hydrotalcite and pure nickel, we have measured by SEM/EDS-X the presence of copper in the powder before and after the reaction. The ratio Cu/Ni in the before sample was 0.07% and in the after sample it was 2.05%. To determine if the copper was due to transmutation of nickel in copper, or to contamination by an unknown source, we did an ICP-MS analysis. The natural ratio ^{63}Cu / ^{65}Cu is 2.2414 while in our experimental measurement it was 2.1915. It is therefore very likely that contamination occurred from an unknown source. It is very unlikely that an unknown reaction produces copper with an isotopic ratio close to the natural one.

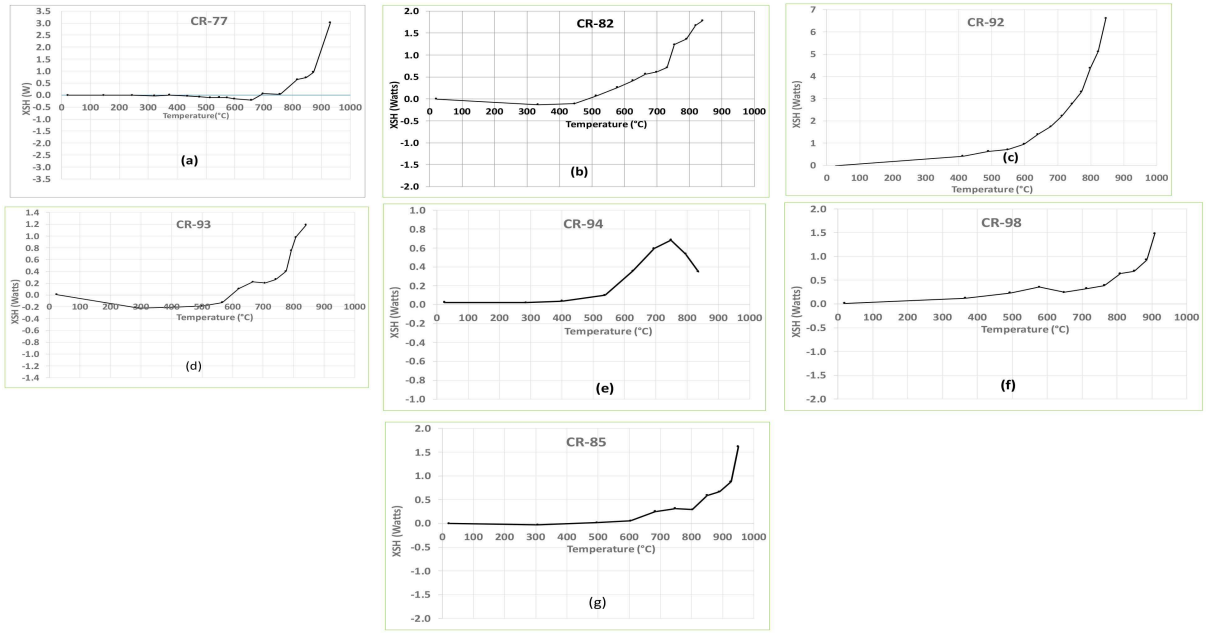

Figure 7. a) CR-77, experiment with hydrotalcite with a ratio Ni-Cu 7/1 (14.6g); b) CR-82, experiment with hydrotalcite with a ratio Ni-Cu 7/1 (30.0g); c) CR-92, experiment with hydrotalcite and pure Ni (52g); d) CR-93, experiment with hydrotalcite and pure Ni (23.3g); e) CR-94, experiment with hydrotalcite and pure Ni (12.6g); f) CR-98, experiment with hydrotalcite and pure Ni (11.9g); g) CR-85, experiment with Ni deposited on C graphite (33.5g).

6. Conclusion

We have shown that using a very precise calorimeter working at high temperatures we have found anomalous excess heat with nano-powders based on nickel alloys produced with hydrotalcites. The amount of heat produced during most of the runs exceeds the amount that can be explained by chemistry. In one experiment that lasted four days, 10 times more energy was produced that could be explained by any chemical reaction. The experiments were performed in hydrogen; we did not try using deuterium. It is important to note that the excess energy is larger during pumping of the hydrogen gas than in the presence of hydrogen at a fixed pressure. The cycling of loading and pumping hydrogen increases the excess energy. This is probably due to the reduction of the metal oxides present at the surfaces of the nano-metals, but also to the modification of the crystal structure of the metal nanoparticles: creation of: dislocations, vacancies, cracks etc. We cannot exclude the role of the interface between the nanoparticles of metals and the aluminum oxide matrix, as pointed out by Biberian et al. [14]. The excess energy is larger at high temperatures when we expect that the loading of hydrogen will decrease, but this is not the case. This behavior has been reported by Iwamura et al. [15] where excess heat is detected when hydrogen flows through multi-layers of nickel/copper at temperatures close to the ones in our experiments.

We have shown in this work the production of anomalous excess power which cannot be explained by chemical reactions. It is therefore tempting to assume that the reaction is of nuclear origin. It has been shown that in reactions with deuterium He-4 is produced at the same ratio as the d+d fusion reaction. With nanoparticles of nickel alloys in hydrogen, the p+p reaction should be much less likely to occur according to theory, so a possible reaction could be

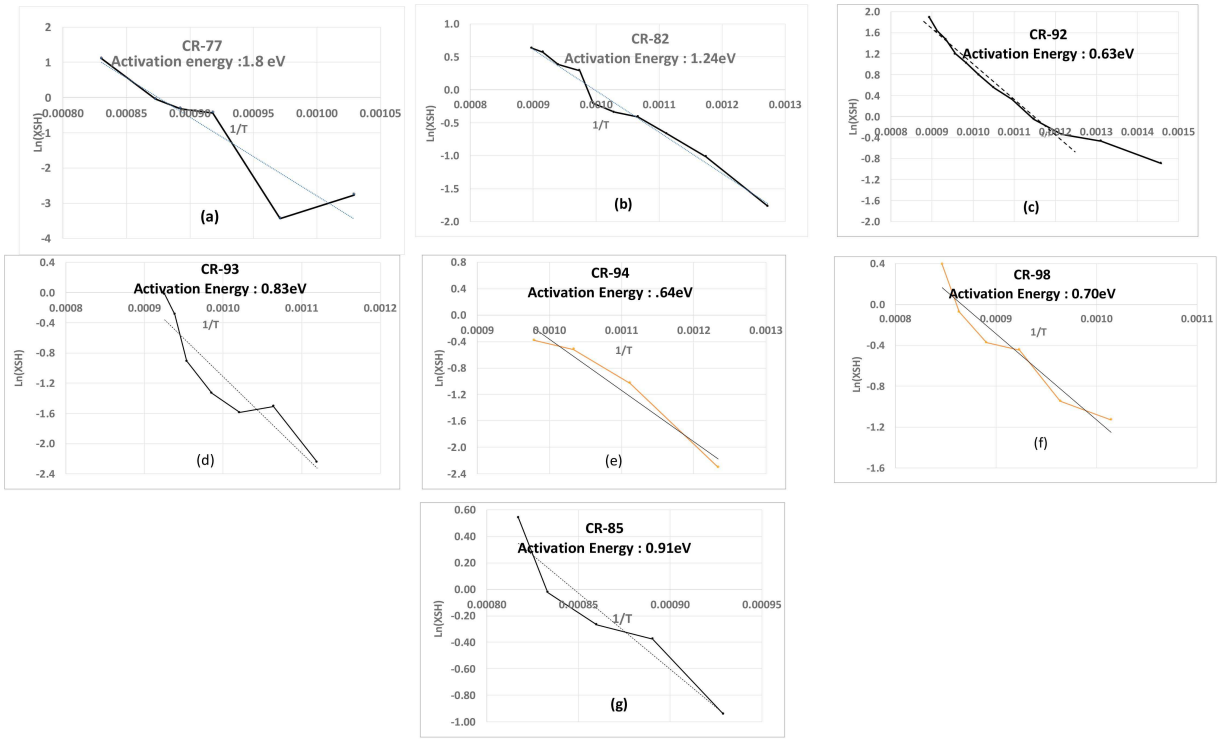

Figure 8. Activation energies for the seven experiments shown in Figure 7 calculated by plotting the logarithm of the excess energy vs 1/T.

between hydrogen and metal atoms. However, Schwinger [16], Takahashi [17] and Storms [18] have proposed other models to explain these reactions with hydrogen. We have shown in this paper that the presence of copper in a pure nickel experiment had an isotopic composition close to the natural one, indicating that this is probably contamination. More work needs to be done to discover the origin of the mechanism that produces the excess heat. For example, it will be interesting to know the loading ratio of hydrogen. This will be done in future experiments.

Acknowledgments

This study is part of the CleanHME project from the European Union's Horizon 2020 research and innovation program under grant agreement No 951974.

References

[1] Arata Y. and Y. Zhang, "*The Establishment of Solid Nuclear Fusion Reactor*", J. High Temp. Soc. 34, 85-93,2008.

[2] Kitamura A., A. Takahashi, K. Takahashi, R. Seto, T. Hatano, Y. Iwamura, T. Itoh, J. Kasagi, M. Nakamura, M. Uchimura, H. Takahashi, S. Sumitomo, T. Hioki, T. Motohiro, Y. Furuyama, M. Kishida, H. Matsune, "*Excess heat evolution from nanocomposite samples under exposure to hydrogen isotope gases*", *International Journal of Hydrogen Energy* **43** (2018) 16187-16200.

[3] Calvet, É. and Prat, H. " *Microcalorimétrie: Applications physicochimiques et biologiques* " Masson, Paris, 1956.

[4] https://en.wikipedia.org/wiki/Calorimeter
[5] https://setaramsolutions.com/app/uploads/sites/2/2020/09/Family-brochure-EN-CALVET.pdf
[6] Schwarz J.A., C.Contescu, A.Contescu - Methods for Preparation of Catalytic Materials - *Chem. Rev. 1995, 95,477-51*
[7] Cavani F., F. Trifiro, A. Vaccari, *Hydrotalcite type anionic clays: Preparations, properties and applications*, **1991**, *Catalysis Today*, 11, 173-301.
[8] Takovite: Mineral information, data and localities. (mindat.org)
[9] Wijitwongwan S., S. Intasa-ard, M. Ogawa, Preparation of layered double hydroxides toward precisely designed hierarchical organization, 2019, ChemEngineering, 3, 68; doi: 10.3390/chemengineering3030068
[10] Fan G., F. Li, D.G. Evans, X. Duan, Catalytic *applications of layered double hydroxides: recent advances and perspectives*, **2014**, *Chem. Soc. Rev.,* 43, pp 7040-7066; doi: 10.1039/c4cs00160e
[11] Huynh H.L., Z. Yu, CO_2 *methanation on hydrotalcite-derived catalysts and structured reactors: A review,* **2020**, *Energy Technol*., 8, 1901475; doi: 10.1002/ente.201901475
[12] He, L. Y. Huang, A. Wang, X. Wang, X. Chen, J.J. Delgado, T. Zhang, *A noble-metal-free catalyst derived from Ni-Al hydrotalcite for hydrogen generation from* $N_2H_4\mathring{u}H_2O$ *decomposition*, **2012**, *Angewandte Chem. Int. Ed*., vol. 51, pp. 6191–6194; doi.org/10.1002/anie.201201737
[13] Smittenberg J., *Absorption of Hydrogen by Nickel*, Nature vol. 133, p. 81, 1934.
[14] Biberian J. P., I. Parchamazad and M. H. Miles, "*Possible Role of Oxides in the* Fleischmann–Pons Effect" J. Condensed Matter Nucl. Sci. 13 (2014) 38–43.
[15] Iwamura Y., J. Kasagi, T. Itoh, T. Takahashi, M. Saito, Y. Shibasaki, and S. Murakami, "*Progress in Energy Generation Research Using Nano-Metal With Hydrogen/Deuterium* Gas", J. Condensed Matter Nucl. Sci. 36 (2022) 285–301.
[16] Schwinger, J. (1990). "*Cold fusion: a hypothesis*." Z. Naturforsch. **45A**: 756.
[17] Takahashi, A. (2004). " $^3He/^4He$ *production ratios by tetrahedral symmetric condensation.*" 11th International Conference on Cold Fusion, Marseilles, France, World Scientific Co.
[18] Storms, E. (2014). "Explaining Cold Fusion." J. Cond. Matter Nucl. Sci. **15**: 295–304.